EJP18 peptide derived from the Juxtamembrane Domain of Epidermal Growth Factor Receptor Represents a Novel Membrane-Active Cell-penetrating Peptide.

Eissa, N.G.[1,2†], Sayers, E.J.[1†], Birch, D.[3†], Patel, S.G.[4], Tsai, Y.-H.[4], Mørck Nielsen, H.[3]* and Jones, A.T.[1]*

1. School of Pharmacy and Pharmaceutical Science, Redwood Building, Cardiff University, Cardiff, CF10 3NB, Wales

2. Current address, Department of Pharmaceutics and Industrial Pharmacy, Faculty of Pharmacy, Zagazig University, Zagazig 44519, Egypt

3. Department of Pharmacy, Faculty of Health and Medical Sciences, University of Copenhagen, Universitetsparken 2, DK-2100 Copenhagen, Denmark

4. School of Chemistry, Cardiff University, Main Building, Park Place, Cardiff, CF10 3AT, Wales

† These authors contributed to this work equally

* Corresponding Authors: Hanne Mørck Nielsen (hanne.morck@sund.ku.dk) and Arwyn T. Jones (jonesat@cardiff.ac.uk)

Abstract

Membrane-active peptides have been extensively studied to probe protein-membrane interactions, to act as antimicrobial agents and cell-penetrating peptides (CPPs) for delivery of therapeutic agents to cells. Hundreds of membrane-active sequences acting as CPPs have now been described including bioportides that serve as single entity modifiers of cell physiology at the intracellular level. Translation of promising CPPs in pre-clinical studies have however been disappointing as only few identified delivery systems have progressed to clinical trials. To search for novel membrane-active peptides a sequence from the EGFR juxtamembrane region was identified (named EJP18), synthesised and examined in its L- and D-form for its ability to mediate the delivery of a small fluorophore and whole proteins to cancer cell lines. Initial studies identified the peptide as being highly membrane-active causing extensive and rapid plasma membrane reorganisation, blebbing and toxicity. At lower, non-toxic concentrations the peptides outperformed the well-characterised CPP octaarginine in cellular delivery capacity for a fluorophore or proteins that were associated with the peptide covalently or via ionic interactions. EJP18 thus represents a novel membrane-active peptide that may be used as a naturally derived model for biophysical protein-membrane interactions or for delivery of cargo into cells for therapeutic or diagnostic applications.

Keywords

Membrane-active peptide, drug delivery, protein delivery, confocal microscopy, flow cytometry, mammalian cell lines

Abbreviations

BSA – Bovine Serum Albumin; CPP – Cell Penetrating Peptide; EGF(R) – Epidermal Growth Factor (Receptor); JM – Juxtamembrane; RTK – Receptor Tyrosine Kinase; CM – Complete Medium; SFM – Serum Free Medium; PBS – Phosphate-Buffered Saline; Rh-tetramethylrhodamine

1. Introduction

The term cell-penetrating peptide (CPP) or protein transduction domain relates to short peptide sequences, usually less than 30 amino acid residues, that have the capacity to deliver themselves and cargo of various forms and sizes to the inside of cells. Since the original discoveries of now well-characterised protein derived CPPs such as Tat and penetratin[1], and synthetic variants such as octaarginine (R8) there has been considerable effort in exploiting their translocating activities for therapeutic and diagnostic purposes[2]. In *in vitro* models these CPPs, and several others, have shown impressive capacity to deliver a range of readout and therapeutic cargo to many cell types, including small molecule drugs or fluorophores and much larger molecules such as nucleotides, peptides, proteins and nanoparticles[3, 4]. Translation of this to effective *in vivo* delivery has however been disappointing and the search continues for novel CPPs or strategic modifications of existing CPPs to improve their delivery performance. CPPs can generally be categorised into three major classes: (i) cationic, such as Tat derived peptides and polyarginines[5], (ii) amphipathic, in which the alterations between cationic and hydrophobic residues give rise to α-helical structures upon membrane interactions[6], e.g. MAP and transportan, and (iii) hydrophobic, such as the PFVYLI sequence[7] and synthetic variants[8]. Additionally, anionic CPPs have also been shown to deliver fluorophores into a range of cell lines[9-11]. It should be noted that in many cases a finite window exists between a CPPs ability to translocate in the absence of cell toxicity and its more global effects on cells in the form of induction of plasma membrane porosity or other indirect effects[12-14].

Cancer cells which overexpress EGFR (ErbB1) have increased activation of downstream signalling pathways driving cell proliferation, survival, angiogenesis, and metastasis[15]. This receptor tyrosine kinase has been targeted using antibodies, antibody-drug conjugates, small molecule drugs and protein-protein interaction inhibiting peptides that act on the phosphorylated cytosolic portion of the receptor to influence its ability to signal[16]. These peptides are often synthesised as CPP chimeras to allow plasma membrane translocation and access of the targeting sequence to the receptor. One example is TE-64562 containing the HIV-Tat_{49-58} peptide sequence (bold) linked to an 18 residue sequence derived from the juxtamembrane (JM) domain of EGFR (**RKKRRQRRRG**-RRRHIVRKRTLRRLLQER)[17]. This EGFR domain region (corresponding to amino acids 645-682 (RRRHIVRKRTLRRLLQEREL-VEPLTPSGEAPNQALLRI) lies immediately downstream of the transmembrane region and harbours a tripartite nuclear localisation sequence (NLS) (**RRR**HIV**RKR**TL**RR,** amino acids 645-657) containing three clusters of basic amino acids (bold)[18]. The JM region itself regulates receptor dimerization, signalling and endocytosis[19, 20]. Our further scrutiny of the EGFR JM region identified three upstream N-terminal amino acids LFM (642-5) that would introduce hydrophobicity to this terminus. Along with a double leucine (658-9) hydrophobic C-terminus, these hydrophobic termini would flank the tripartite NLS and produce the 18 amino acid sequence 642-LFMRRRHIVRKRTLRRLL**-**659. As an unmodified peptide, it would have a mass of 2421.0 Dalton, an isoelectric point of 12.88, and a net charge of 8.1 at pH 7.0 (pepcalc.com). Our interest in this sequence stems from the fact that in this natural sequence located at the cytosolic/plasma membrane interface, the cationic (hydrophilic) residues are spaced between hydrophobic residues. Based on other CPP sequences and findings that terminal hydrophobicity of CPPs influences peptide-cell interactions[21, 22], it was hypothesised that this peptide, that we term **E**GFR **J**uxtamembrane **P**eptide-18 (EJP18) may have CPP activity and EGFR dependant cytotoxicity when added to cells and thus act as a bioportide[23].

In this study we demonstrate that EJP18 can be classified as a novel CPP having the capacity to effectively deliver a fluorophore and proteins to cells whether as non-covalent complexes or covalently in frame after expression in *E. coli.* At higher concentrations the membrane activities of L-EJP18 and especially D-EJP18 were pronounced, manifested as rapid and extensive plasma membrane blebbing and damage in cells independent of their EGFR expression. Analysis of the JM regions of other receptor tyrosine kinases in the human genome reveal that several may contain interesting sequences with cell penetrating capacity.

2. Materials and Methods

2.1. Chemicals and reagents

All peptides used in this study (Table 1), were purchased from EZBiolab (Parsippany, NJ, USA). Cell culture media, serum, trypsin, Hoechst 33342 (#H3570), bovine serum albumin (BSA)-Alexa647 (#A13100), BSA-Alexa488 (#A34785), dextran-Alexa488 (#D22910) were purchased from Fisher Scientific (Loughborough, UK). Agarose, Mini-PROTEAN® TGXTM gels 10% (#456-1033), Clarity Western Enhanced Chemiluminescence substrate, sodium dodecyl sulphate (SDS), precision plus protein dual colour standards were obtained from Bio-Rad (Watford, UK). Horseradish peroxidase (HRP) conjugated mouse anti-β-tubulin (#AB21058) was purchased from Abcam (Cambridge, UK). Rabbit anti-EGFR (#HPA018530) was from Sigma (Gillingham, UK) and goat anti-rabbit HRP (#32460) was from Fisher Scientific. DRAQ7^{TM} (#DR71000) was from Biostatus (Leicestershire, UK) and CellTiter–Blue® viability reagent was purchased from Promega (Southampton, UK).

DMEM, RPMI 1640, 0.05% Trypsin-EDTA were all obtained from Life Technologies (Fisher Scientific). Phosphate-buffered saline (PBS) was made in house and buffered to pH7.4.

All peptides and protein conjugates used in this study are described in Table 1.

2.2. eGFP-CPP conjugates

Plasmids pEV eGFP and pEV eGFP-R8 were described previously[24]. To construct plasmid pEV eGFP-EJP18, the vector for the plasmid was PCR-amplified from pEV eGFP with primers TAGGAATTCAAGCTTAAGCTGAGCAATAACTAGC and CCATGTGGTGGTGGTGGTGGT-GCATATGTATATCTC, the insert for the plasmid was PCR- amplified from pEV eGFP with primers CCACCACCACCACCACATGGTGAGCAAGGGCGAG and AGCTTAAGCTTGAAT-TCCTACAGCAGGCGGCGCAGGGTGCGTTTGCGCACAATATGGCGGCGGCGCATAAACA GCTTGTACAGCTCGTCCATGCCGAG. The two PCR fragments were joined together by Gibson assembly to afford the desired plasmid. The nucleotide sequences encoding eGFP-EJP18 and the corresponding amino acid sequence are shown in the Supplementary Information. Characterisation data can be found in Supplementary Information, Figures S1 and S2. Recombinant eGFP, eGFP-R8 and eGFP-EJP18 proteins were expressed and purified as previously described [25].

2.3. Cell culture

HeLa, human cervical carcinoma, cells (ATCC, Middlesex, UK), MCF-7 and MDA-MB-231, both breast cancer cells (ATCC), and A431 epidermal cancer cells (School of Dentistry, Cardiff University) were maintained in a humidified 5% CO_2 37 °C incubator in DMEM supplemented with 10% foetal bovine serum (FBS). Human acute myeloid leukaemia KG1a cells (ECACC, Porton Down, UK) were maintained as a suspension in RPMI 1640 medium supplemented with 10% FBS. Herein medium supplemented with FBS are termed complete media (CM). Each adherent cell line was sub-cultured after 3-5 days of growth, at 70-90% confluency. KG1a cells were passaged at confluencies between 2 – 5 x10^5 cells/mL. All cell lines were routinely tested for mycoplasma contamination and confirmed negative.

2.4. Cell viability studies

To account for different growth rates, cells were seeded in black 96-well plates at densities that provided 80-90% confluency after 24 h; KG1a cells (1.5×10^4 cells/well), HeLa (8×10^3 cells/well), MCF-7 (2.5×10^3 cells/well), MDA-MB-231 (2×10^3 cells/well) and A431 (2×10^3 cells/well) in a total volume of 100 µL. After a minimum of 24 h, cells were treated with peptides in CM for 24 h. Viability studies were conducted using the CellTiter-Blue® assay where cells were incubated with 100 µL peptide in CM for 20 h and additionally for 4 h with 20 µL of CellTiter-Blue® reagent added prior to measurements. Samples were read on a FLUOstar Optima fluorescent plate reader (Ex. 584nm, Em. 612nm) and viability determined after background subtraction by comparison to a vehicle control.

2.5. Determination of EGFR levels in cancer cell lines

For adherent cell lines (HeLa, A431, MCF-7 and MDA-MB-231), cells were grown to approximately 70% confluency in T-75 tissue culture flasks. The medium was aspirated, and the cells were washed three times with PBS. Ice cold lysis buffer 0.5 mL (50 mM NaCl, 50 mM Tris base pH 8.0, 1% Nonidet p-40 [Sigma Aldrich, Gillingham, UK] plus cOmplete Mini protease inhibitors [Roche, Burgess Hill, UK]) was added on ice and the cells were scraped from the flask surface. The flask content was transferred to an Eppendorf tube and kept on ice for 5-15 min, then centrifuged (13,800 × *g*, 4 ºC) for 15 min, prior to removing the supernatant to a clean Eppendorf tube. For the non-adherent KG1a cells, the total volume of a T-75 flask was transferred to a 15 mL centrifuge tube,

centrifuged at 900 × *g* for 2 min and then resuspended in 5 mL fresh CM. A volume containing 1 x 10^6 cells was pelleted by centrifugation at 900 x *g* and resuspended in PBS, washed again in PBS before resuspending the pellet in ice cold lysis buffer (620 µL). After 5-15 min, the sample was centrifuged (13,800 × *g*, 4 ºC) and the supernatant was harvested. For all cell lines, following lysate collection and protein quantification via the BCA assay (Fisher Scientific), 20 µg of protein was loaded and run (100 V, 60 min) on a 10% precast gel (Bio-Rad). Proteins were transferred to polyvinylidene fluoride membranes (Immobilon-P transfer membrane, Fisher Scientific) and EGFR was detected via immunoblotting (anti-EGFR Ab diluted 1:1000 in 2% milk/PBS/0.2% Tween [Sigma Aldrich] and incubated overnight). Samples were washed 3X for 5 min in PBS/0.2% Tween and incubated with the secondary antibody (1:1000 in 2% milk/PBS/0.2% Tween), after further washing of 3X 5 min in PBS/0.2% Tween, membranes were incubated with Clarity ECL reagent and luminescence detected using a ChemiDoc system (Bio-Rad).

2.6. Cell morphology studies

HeLa cells, MDA-MB-231 and A431 cells were seeded in imaging dishes (2.5×10^5, 1.8×10^5 and 2.5×10^5 cells per dish, respectively) and allowed to adhere overnight. Just prior to experimentation, the cells were washed three times with serum free media (SFM). In addition, 5×10^5 KG1a cells were collected in an Eppendorf tube and centrifuged (400 × *g*, 3 min) before being resuspended in SFM and transferred to an MatTek imaging dish (Ashland, MA). Peptide solutions (L-EJP18 or D-EJP18 in a final concentration of 20 µM in 200 µL SFM containing 1 µL DRAQ7™) were then added to the cells. Cells were kept on a humidified stage (5% CO_2, 37ºC) and imaged by confocal microscopy using the 633 nm laser with a 63× 1.4NA objective. Images were acquired at 30 s intervals over 1 h. Images were processed using ImageJ software[26].

2.7. Confocal microscopy of Rh-CPP, eGFP-CPP and CPP:BSA complexes

HeLa cells and MDA-MB-231 cells were seeded at a density of 1.8×10^5 cells per imaging dish and allowed to adhere overnight under tissue culture conditions. The next day, where applicable, cell lysosomes were labelled by incubating the cells with 100 µg/mL 10 kDa dextran-Alexa488 (Dex488) or 10 kDa dextran-Alexa647 (Dex647, both Fisher Scientific) for 2 h in CM under tissue culture conditions. Subsequently, cells were washed three times with CM and incubated for 12-14 h to chase the dextran into the lysosomes[27, 28].

On the day of experiment, cells were washed with SFM and incubated with either Rh-CPP, eGFP-CPP or CPP:BSA complexes in SFM for 1 h, 37 °C 5% CO_2. Complexes were formed containing 8 µM CPP and 240 nM BSA-Alexa647 (BSA647) in nuclease free distilled water for 30 min at room temperature following a protocol based on Sayers et al.[29]. Following this the complexes were diluted 1:3 with SFM giving final CPP and BSA concentrations of 2 µM and 60 nM respectively and incubated with the cells for 1 h under tissue culture conditions. For pulse-chase peptide experiments in cells (Figure 6), lysosome labelled cells were washed in CM and re-incubated for 1 h before imaging. Where low temperature experiments were performed, cells were pre-chilled on ice (4 °C) for 15 min before washing and incubating with prechilled Rh-CPP in SFM for 1 h. Here, cells were washed and imaged in pre-chilled imaging medium.

After the incubation period, cells were washed with imaging medium (phenol red free DMEM supplemented with 25 mM HEPES pH 7.4 and 10% FBS) and finally imaged in imaging medium containing Hoechst 33342 (10 µg/mL) and analysed on a Leica SP5 confocal microscope (63x 1.4 N.A. objective using 405 nm, 488 nm or 543 nm and 633 nm lasers with a 95.5 µm pinhole, pixel size is 283 nm, using Leica Type F immersion oil). Sequential scanning was used to separate overlapping emission profiles. All cell imaging was performed in live cells at 37 °C, 5% CO_2, 90% humidity over the course of the experiment apart from low temperature uptake studies that were imaged in ice cold imaging medium.

2.8. Flow cytometry analysis of Rh-CPP, eGFP-CPP and CPP:BSA complexes

HeLa cells and MDA-MB-231 cells were seeded at a density of 1×10^5 cells per well in 12-well plates so that they were 80-90% confluent on the day of experiment. On the day of experiment, the medium was aspirated, and the cells were washed with SFM and then incubated under tissue culture conditions for 1 h with test compounds (L-EJP18, D-EJP18 or L-R8 at 1-5 µM in SFM) either as Rh-labelled conjugates, or as BSA647 complexes prepared as above. The experiment was repeated at 4 °C for the Rh-labelled conjugates at 2 µM. Following 1 h of exposure, the test compounds were removed, and cells were washed with ice-cold PBS and then detached with trypsin at 37 °C. The trypsinisation was terminated by addition of ice-cold CM, and the cell suspensions were collected in Eppendorf tubes and centrifuged (270 × g, 4 °C, 4 min). The supernatant was removed and the cells were washed with ice-cold heparin sulphate (Sigma Aldrich, diluted 20 µg/mL in PBS) before being centrifuged again under the same conditions and resuspended in ice-cold CM. Hereafter, the cells were kept on ice before analysis on a Gallios flow cytometer (Beckman Coulter, Fullerton, CA, USA).

At least 5000 viable cells were counted, using gating for front- and side scattering. Rh-labelled EJP18 and BSA-Alexa647 were detected using red and far-red filters.

2.9. Data analysis

The IC_{50} values for EJP18 towards each cell line were calculated using GraphPad Prism (GraphPad Software, La Jolla, CA, USA) and the Hill equation (shown below), as described by Birch *et al*. [30].

$$Relative\ viability\ (\%) = \frac{Top - Bottom}{1 + 10^{(LogIC_{50} - Log[CPP]) \times Hill\ slope}}$$

In order to prevent erroneous calculations as a result of autophagocytosis, the top of the curve was constrained at 100 % viability.

Data were compared with a one-way ANOVA combined with a Tukey's multiple comparison analysis using GraphPad Prism.

3. Results

Both L- and D-forms of the EJP18 peptide were initially tested against four cancer cell lines from a range of tissues to determine the effects of the L (Figure 1A) and D (Figure 1B) forms on cell viability (Table 2). Both showed little toxicity below 10 μM when incubated with cells for 24 h and above this concentration the different cell lines had varied sensitivities. In the skin epithelial A431 cell line only limited toxicity was observed to the L enantiomer (IC50 > 100 μM) and moderate toxicity against the D enantiomer (IC50 ~ 22 μM). In contrast, the acute myeloid leukaemia cell line KG1a showed the highest susceptibility to L-EJP18 with toxicity only marginally higher when exposed to the D enantiomer (IC50 20 vs 15 μM). The cervical epithelial HeLa line showed a much higher level of sensitivity to the D over the L form of the peptide giving IC50 values of 63 μM vs 12 μM, respectively. Mammary epithelial line MDA-MB-231 proved the most resistant to toxicity from D-EJP18, with an IC50 approximately half the value than when incubated with L-EJP18.

To determine if there was any relationship between toxicity of our peptide and EGFR expression levels, protein normalised EGFR expression was tested by western blot. Both A431 and MDA-MB-

231 cell lines showed high EGFR expression while HeLa and KG1a, respectively, produced low and undetectable levels of this protein. This is in agreement with mRNA expression profiles from 'The Human Protein Atlas' and the 'Cancer Cell Line Encyclopaedia' (CCLE) for HeLa, MDA-MB-231 and A431 cells[31, 32], and no EGFR data could be identified for KG1a cells. The high EGFR expressing cell line, A431, had the lowest L-EJP18 toxicity and the lowest EGFR expressor, KG1a, had the highest L-EJP18 toxicity. MDA-MB-231 and HeLa cells have similar toxicity profiles and D-EJP18, showed no correlation between EGFR expression and toxicity.

Using live cell time lapse confocal microscopy, we have previously shown that some cationic toxic peptides very rapidly cause large protrusions to emanate from the plasma membrane immediately prior to evidence of membrane damage and porosity to dyes such as propidium iodide[7, 21]. Focusing on a high EGFR expressor (MDA-MB-231), a low expressor (HeLa) and the previously tested suspension cell line KG1a, we evaluated their immediate responses to 20 μM of both EJP18 enantiomers in comparison with r8-PAD (rrrrrrrrGGklaklakklaklakGC) that we previously showed to be extremely plasma membrane-active and toxic at 20 μM[7]. Cells incubated with the peptides were imaged by time-lapse microscopy every 30 s for 1 h in the presence of DRAQ7, a marker for membrane permeability, and the results are shown as movies M1-M12 (Supplementary Information); the 1 h time point is shown in Figure 2. The movies clearly demonstrate very rapid high plasma membrane activity of r8-PAD producing large blebs on the surface of all three cell lines before showing the first signs of porosity to DRAQ7 between 5 min and 10 min; within 1 h all cells were DRAQ7 positive. KG1a cells incubated with the EJP18 enantiomers also showed rapid and extensive 'blebbing' of the plasma membrane with D-EJP18 (Supplementary Information, M11) producing blebs on the surface within 25 min compared to 40 min for L-EJP18 (Supplementary Information, M10). Despite this, the cells were not strongly positive for DRAQ7 with weak dye signals identified in a minority of cells after 1 h. MDA-MB-231 cells showed minor membrane disturbance when incubated with both enantiomers and remained DRAQ7 negative throughout the 1 h period (Supplementary Information, M6 and M7). Membrane protrusions were visible for both enantiomers of peptide when incubated with HeLa cells (Supplementary Information, M2 and M3), and those incubated with D-EJP18 showed evidence of membrane porosity. Overall, these time lapse experiments reflect the data seen in the 24 h viability assays (Figure 1) and noticeable is that the HeLa cell line is much more susceptible to the D-enantiomer over the L-enantiomer.

As the peptides clearly showed plasma membrane activity, we analysed their ability to carry a fluorescent model small molecule ([tetramethyl]rhodamine, Rh) and protein cargos (albumin and eGFP) to MDA-MB-231 and HeLa cells at 1-5 μM. Cells were incubated with L- and D-Rh-EJP18 for 1 h and analysed by live cell confocal microscopy and flow cytometry, along with Rh-L-R8 representing a very well characterised CPP[33, 34]. At 2 μM all three peptides were visible in vesicular structures in both cell lines (Figure 3A and B). Intensity of these vesicles was most prominent in HeLa incubated with Rh-L-EJP18. Fluorescence from both Rh-EJP18 enantiomers and Rh-L-R8 was punctate-scattered in the cytoplasm with some enrichment in a juxtanuclear region; similar subcellular distribution of fluorescence was observed in MDA-MB-231 cells. For both these cell lines there was little colocalisation of either enantiomer with Transferrin-Alexa488 (a marker for early and recycling endosomes) following a 1 h pulse (Supplementary Information, Figure S4).

Incubating cells on ice with 2 μM Rh-peptides (Table 1) for 1 h produced no visible fluorescence (data not shown). Increasing peptide concentration to 10 μM showed little internalised fluorescence of either Rh-EJP18 peptide with a minority of cells showing small plasma membrane bound aggregates (Supplementary Information, Figure S5). As seen previously using L-R8-Alexa488[33], Rh-L-R8 gives cytosolic and nuclear labelling when incubated at high concentrations (here 10 μM) at 4 °C in serum free medium. This highlights that uptake of EJP18 peptides can only occur in the presence of energy and unlike L-R8 the sequence cannot directly translocate through the plasma membrane at 4 ˚C.

We then used flow cytometry to quantify peptide uptake and at 1 μM, in both cell lines, cell-associated fluorescence was significantly higher ($P<0.001$) for Rh-D-EJP18 compared with Rh-L-EJP18 or Rh-L-R8 for both cell lines (Figure 3C-D). Morphological effects in cells incubated with higher concentrations of Rh-D-EJP18 resulted in the majority of cell counts falling outside of the gated region (data not shown) and a reliable fluorescence intensity reading for these concentrations could not be obtained. Uptake levels were similar between Rh-L-EJP18 and Rh-L-R8 at 2 μM and 5 μM ($P>0.05$).

Cell-penetrating peptides have been shown to deliver proteins to cells as non-covalent complexes or CPP-fusions expressed in *E. coli* and purified[25, 35-38]. Enhanced green fluorescent protein (eGFP) was selected as a model protein and synthesised in frame with EJP18 and purified as an eGFP-EJP18 conjugate. Its cellular uptake was analysed by microscopy in comparison with eGFP-R8 in HeLa

(Figure 4A) and MDA-MB-231 cells (Figure 4B). For both cell lines there was appreciably higher visible cell-associated fluorescence after incubation with 2 μM eGFP-EJP18 than eGFP-R8, with eGFP alone showing no observed fluorescence under these microscopy settings. While cells incubated with Rh-EJP18 showed only punctate endosomal fluorescence after 1 h, eGFP-EJP18 was present as punctate vesicular fluorescence but also ~~clearly~~ labelled the plasma membrane. Labelling the plasma membrane of both cell lines showed, in addition to endocytic structures, aggregation of the protein-peptide conjugate at or very close to the plasma membrane after 1 h of incubation (Supplementary Information, Figure S6). Brightness enhancing the eGFP-R8 images incubated with both cell lines allowed us to more easily determine these subcellular localisations (Supplementary Information, Figure S7). In both cell lines eGFP-R8 was located to small scattered vesicles.

To assess the capacity of EJP18 to internalise protein as non-covalent CPP:protein complexes, the peptides were mixed with fluorescent BSA647 at a molar ratio of 100 to 3 before adding to cells as CPP:BSA647. L-R8 and L-EJP18 failed to enhance BSA647 internalisation above background levels in either HeLa or MDA-MB-231 cells at any of the tested concentrations (Figure 5). However, D-EJP18 proved successful in internalising significant amounts of this protein at 2 μM localising to scattered vesicles in a similar pattern seen with the Rh-EJP18 peptides. This high uptake was mirrored by flow cytometry where, at the lowest concentration, D-EJP18 was able to internalise significantly higher amounts of BSA647 than the other peptides in both cell lines and values for D-EJP18:BSA647 exceeded values obtained when the other peptides were at five times higher concentrations. It should be noted that, similar to results seen for the rhodamine constructs, D-EJP18:BSA647 produced morphological changes at 2 and 5 μM that shifted HeLa and MDA-MB-231 outside of the gated region after preparation for flow cytometry. In Hela cells there were no significant differences in the uptake of BSA647 by either L-EJP18, L-R8 or without peptide complexation. In MDA-MB-231 cells, 1 μM D-EJP18 internalised significantly more BSA than the L-enantiomer; and notably, in this cell line L-R8 outperformed L-EJP18 at low concentrations (1 or 2 μM), however, at 5 μM they were statistically equivalent.

To further explore the endocytosis of EJP18-cargo, we investigated whether, once internalised, they trafficked by endocytosis to lysosomes. For these experiments lysosomes were labelled via a short pulse and overnight chase with fluorescent dextran that is known to traffic to these organelles via Rab7a labelled late endosomes[27]. This then allowed for subsequent analysis of the intracellular delivery of the EJP18 conjugates to these organelles in HeLa and MDA-MB-231 after a short one

hour 'pulse' incubation (Figure 6). HeLa incubated with Rh-labelled D- or L-EJP18 showed a moderate level of colocalisation between with the probe and lysosomes. In both cases fluorescent peptide was scattered throughout the cell. A similar level of colocalisation and distribution was seen with EJP18:BSA647 complexes. In contrast, MDA-MB-231 incubated with either Rh-EJP18 or EJP18:BSA647 showed low levels of colocalisation indicating that either the peptide/protein complexes trafficked differently in this cell line, or the overall rate of trafficking to the lysosome was much slower. Interestingly both the Rh-EJP18 and EJP18:BSA complexes seemed to localise to a similar juxtanuclear region containing dextran labelled-lysosomes; that in this cell line also harbours EEA1-labelled early endosomes and LAMP-1-labelled lysosomes[39, 40]. Both HeLa and MDA-MB-231 incubated with eGFP-EJP18 showed no colocalisation with lysosomes. In both cases fluorescence was limited to puncta at the periphery of the cell indicating that further internalisation of this fraction to the lysosomal system is relatively slow.

4. Discussion

Our time lapse microscopy experiments clearly highlighted the capacity of both EJP18 enantiomers to affect plasma membrane integrity at concentrations higher than 10μM. Based on this and the collected viability data together with EGFR expression analysis it is very unlikely that EJP18 toxicity is linked to the expression of this receptor. This suggests that the peptide has an alternative mechanism for inducing cell toxicity that most probably lies at the level of the plasma membrane. EGFR levels were predictive of the toxicity of another EGFR JM derived peptide conjugated to $Tat_{49\text{-}58}$ (TE-64562) [17]. Cell lines that expressed moderate to high EGFR were more susceptible to TE-64562 and there was no toxicity (up to 100 μM) or delivery capacity associated with the JM sequence alone (RRRHIVRKRTLRRLLQER). Noted is that this sequence, like that of EJP18 is also composed of 18 residues however at the N- and C terminus lie cationic residues. This strongly supports our initial hypothesis that hydrophobic termini aid membrane interaction. However, it is very difficult to refute the possibility that the JM cargo peptide in TE-64562 had a significant influence on the capacity of $Tat_{49\text{-}58}$ to enter cells. In support of this finding, a very short threonine phosphorylated peptide termed T654 from this JM of EGFR (Ac- RKRT^{P}LRRLK-fluorescein) entered cells and inhibited irradiation-induced nuclear localization of EGFR[41]. However, uptake was monitored after 16 h and it is very difficult to determine its subcellular localization. More recently a peptide consisting of a pH

dependent membrane spanning sequence (pHLIP) in frame with a very short EGFR JM sequence 654-TLRRLLQ-660 was shown to inhibit EGRF dimerization, inhibit cell migration and induce cytotoxicity and downstream effects[42]. It would be interesting to determine whether this shorter peptide influences the membrane spanning capacity of pHLIP or whether EJP18 could also be active in this way attached to pHLIP to give higher selectivity. While there were no links between EGFR expression and EJP18 induced toxicity, the peptide may be having some effects on receptor dimerisation and/or activation, similar to those seen with TE64562, T654 and pHLIP-JMA[17, 41, 42]. To interact with the EGFR JM domain, as initially predicted, would require crossing the plasma membrane to reach the target. While there was little evidence of cytosolic delivery, we cannot refute the possibility that a very low fraction, beyond the limit of detection of our assay, was able to perform this feat.

The general increased toxicity of the D- versus L-EJP18 is likely to be due to degradation of the latter by proteases that are known to have significant effects on CPP translocation activities [43]. These may be present in the serum as a purchased product or may be released from cells during the incubation stages. Thus the effective concentration of D- versus L- forms are maintained for a longer period to mediate effects[44]. This is corroborated by similar studies on the exposure of penetratin to Caco-2 cells, in which intact D-penetratin elicited more detrimental effects than the corresponding L form [45].

The mechanism by which these peptides cause such profound membrane disruption is unknown and also unknown is whether pores are initially formed before physical blebbing and DRAQ7 staining can be observed. These observations are similar to the effects on mammalian cells of equivalent concentrations of the extensively studied pore forming bee venom toxins melittin and mastoparan[46, 47]. Interestingly, four of the five cationic residues on the 26 residue melittin (GIGAVLKVLTTGLPALISWIKRKRQQ) are localized together at the C-terminus whilst two of the three same residues in mastoparan also are localized at the C-terminus (INLKALAALAKKIL). Both these peptides have toxic effects on mammalian and eukaryotic cells is thought to be induced by the formation of pores in membranes [48]; other membrane interacting effects have also been noted[49]. It remains to be determined whether the interaction of these peptides with membranes is similar to that of EJP18 with its cationic residues spaced throughout the sequence, flanked by two hydrophobic residues at each end. The presence of punctate spots on (or adjacent to) the plasma membrane suggests the occurrence of oligomerisation. It has been noted that peptide dimers of the amphiphilic peptide,

LK-3, induced further oligomerisation and the burying of their hydrophobic motifs in the plasma membrane to aid internalisation [50].

Overall EJP18 managed to deliver a small-molecule fluorophore and macromolecular protein cargoes covalently attached via a peptide bond or as non-covalent protein:peptide complexes. There is still significant interest in delivering proteins to cells by CPPs to mediate a biological response interest or for delivery across a biological barrier[37, 51]. The eGFP-EJP18 protein conjugate appeared to aggregate on the plasma membrane of the cell. However, further scrutiny clearly identified endocytic uptake as well as association with different regions of the plasma membrane. However, when the peptide was complexed with BSA there was clear signs that endocytosis was occurring and this was marked by very different eGFP-EJP18 and EJP18:BSA localisation after a 1 h pulse – 1 h chase. Interestingly both the Rh-EJP18 and EJP18:BSA complexes seemed to localise to a similar juxtanuclear region containing dextran labelled-lysosomes; that in this cell line also harbours EEA1-labelled early endosomes and LAMP-1-labelled lysosomes[39, 40]. Our initial experiments with the Rh-conjugated peptides and transferrin suggests little or no involvement of clathrin mediated endocytosis as an uptake process and this warrants further analysis. For all studies presented here there was little evidence that either L- or D-EJP18 was able to promote delivery of fluorophore or protein to the cytosol of cells but and small fraction that may escape through the plasma membrane of endosomal membrane is extremely difficult to detect by fluorescence microscopy.

The EJP18 sequence was derived from the JM of EGFR, a member of the ErbB family of signalling receptors that, in humans, form the larger 58-member receptor tyrosine kinase family[52]. Within the JM region there are some interesting and notable sequence conservation that is predicted to influence function through interactions with negatively charged lipids[52]. Of interest is the fact that the JM regions of many RTKs are rich in positively charged residues suggesting that other potential CPPs may be hidden within this family of proteins (Table 3). This hypothesis remains to be tested.

5. Conclusions

Peptides such as melittin and mastoparan have been extensively studied as models of protein-membrane interaction and EJP18 can be seen as a new member of this family. As a natural membrane interacting region within EGFR, this sequence interacts with phosphatidylinositol 4,5 bisphosphate

(PIP_2) and other phospholipids on the inner leaf of the membrane[53]. Further information on EJP18 membrane interaction may be gleaned from studies with artificial membranes containing PIP_2 that has been shown to mediate the oligomerisation of antimicrobial defensin peptides leading to cytotoxicity[54, 55]. At concentrations greater than 10 μM L- and D-EJP18 are highly membrane-active and differentially toxic to the cell lines studied here. There remains significant interest in cytotoxic peptides and their derivatives as anti-cancer agents and delivery vectors[56] and EJP18 may in the future fall into this category. A clear overlap between sequences of cell-penetrating and antimicrobial peptides has been noted[57, 58] and it remains to be determined whether our sequence also has activity against prokaryotes and fungi. At low concentrations, the EJP18 sequences were at least as effective as L-R8 in delivering a fluorophore and proteins to cells thus allowing for their classification as novel CPP. This merits further analysis of whether their translocation activities can be exploited to deliver a therapeutic cargo across a biological barrier to mediate a physiological response.

6. Acknowledgments

We would like to thank Anders Davidsen for performing some preliminary experiments with the peptide.

7. Declarations of Interest

All authors declare no competing interests.

8. Funding

This work was supported by funding from the Egyptian Ministry of Higher Education (NGE/ATJ), the Danish Council for Independent Research, Technology and Production Sciences (grant no. 4005-00455), (DB/HMN), Novo Nordisk Foundation (Grand Challenge Programme; NNF16OC0021948) (DB/HMN) and Innovative Medicines Initiative Joint Initiative under grant agreement n° 115363 resources composed of financial contribution from the European Union's Seventh Framework Programme (FP7/2007-2013) and EFPIA companies (EJS/HMN/ATJ).

9. Author Contribution Statement

NGE, EJS, DB, HMN and ATJ were all involved with the design of the experiments run by NGE, EJS and DB. SGP designed and manufactured the eGFP-CPPs with guidance from YHT. NGE, EJS, DB, and ATJ were all involved with writing the manuscript. All authors were involved in editing the manuscript and approve its publication.

10. References

1 Copolovici, D. M., Langel, K., Eriste, E. and Langel, U. (2014) Cell-penetrating peptides: design, synthesis, and applications. ACS Nano. **8**, 1972-1994
2 Tripathi, P. P., Arami, H., Banga, I., Gupta, J. and Gandhi, S. (2018) Cell penetrating peptides in preclinical and clinical cancer diagnosis and therapy. Oncotarget. **9**, 37252-37267
3 Silva, S., Almeida, A. J. and Vale, N. (2019) Combination of Cell-Penetrating Peptides with Nanoparticles for Therapeutic Application: A Review. Biomolecules. **9**
4 Habault, J. and Poyet, J. L. (2019) Recent Advances in Cell Penetrating Peptide-Based Anticancer Therapies. Molecules. **24**
5 Milletti, F. (2012) Cell-penetrating peptides: classes, origin, and current landscape. Drug Discov Today. **17**, 850-860
6 Fernandez-Carneado, J., Kogan, M. J., Pujals, S. and Giralt, E. (2004) Amphipathic peptides and drug delivery. Biopolymers. **76**, 196-203
7 Watkins, C. L., Brennan, P., Fegan, C., Takayama, K., Nakase, I., Futaki, S. and Jones, A. T. (2009) Cellular uptake, distribution and cytotoxicity of the hydrophobic cell penetrating peptide sequence PFVYLI linked to the proapoptotic domain peptide PAD. J Control Release. **140**, 237-244
8 Schmidt, S., Adjobo-Hermans, M. J., Kohze, R., Enderle, T., Brock, R. and Milletti, F. (2017) Identification of Short Hydrophobic Cell-Penetrating Peptides for Cytosolic Peptide Delivery by Rational Design. Bioconjug Chem. **28**, 382-389
9 Martin, I., Teixido, M. and Giralt, E. (2011) Design, synthesis and characterization of a new anionic cell-penetrating peptide: SAP(E). Chembiochem. **12**, 896-903
10 Jones, A. T. and Sayers, E. J. (2012) Cell entry of cell penetrating peptides: tales of tails wagging dogs. J Control Release. **161**, 582-591
11 Yamada, T., Signorelli, S., Cannistraro, S., Beattie, C. W. and Bizzarri, A. R. (2015) Chirality switching within an anionic cell-penetrating peptide inhibits translocation without affecting preferential entry. Mol Pharm. **12**, 140-149
12 Saar, K., Lindgren, M., Hansen, M., Eiriksdottir, E., Jiang, Y., Rosenthal-Aizman, K., Sassian, M. and Langel, U. (2005) Cell-penetrating peptides: a comparative membrane toxicity study. Anal Biochem. **345**, 55-65
13 Dowaidar, M., Gestin, M., Cerrato, C. P., Jafferali, M. H., Margus, H., Kivistik, P. A., Ezzat, K., Hallberg, E., Pooga, M., Hallbrink, M. and Langel, U. (2017) Role of autophagy in cell-penetrating peptide transfection model. Sci Rep. **7**, 12635
14 Kloss, A., Henklein, P., Siele, D., Schmolke, M., Apcher, S., Kuehn, L., Sheppard, P. W. and Dahlmann, B. (2009) The cell-penetrating peptide octa-arginine is a potent inhibitor of proteasome activities. Eur J Pharm Biopharm. **72**, 219-225
15 Sigismund, S., Avanzato, D. and Lanzetti, L. (2018) Emerging functions of the EGFR in cancer. Mol Oncol. **12**, 3-20

16 Yewale, C., Baradia, D., Vhora, I., Patil, S. and Misra, A. (2013) Epidermal growth factor receptor targeting in cancer: a review of trends and strategies. Biomaterials. **34**, 8690-8707
17 Boran, A. D., Seco, J., Jayaraman, V., Jayaraman, G., Zhao, S., Reddy, S., Chen, Y. and Iyengar, R. (2012) A potential peptide therapeutic derived from the juxtamembrane domain of the epidermal growth factor receptor. PLoS One. **7**, e49702
18 Hsu, S. C. and Hung, M. C. (2007) Characterization of a novel tripartite nuclear localization sequence in the EGFR family. J Biol Chem. **282**, 10432-10440
19 Hubbard, S. R. (2009) The juxtamembrane region of EGFR takes center stage. Cell. **137**, 1181-1183
20 Jura, N., Endres, N. F., Engel, K., Deindl, S., Das, R., Lamers, M. H., Wemmer, D. E., Zhang, X. and Kuriyan, J. (2009) Mechanism for activation of the EGF receptor catalytic domain by the juxtamembrane segment. Cell. **137**, 1293-1307
21 Watkins, C. L., Sayers, E. J., Allender, C., Barrow, D., Fegan, C., Brennan, P. and Jones, A. T. (2011) Co-operative membrane disruption between cell-penetrating peptide and cargo: implications for the therapeutic use of the Bcl-2 converter peptide D-NuBCP-9-r8. Mol Ther. **19**, 2124-2132
22 Takayama, K., Nakase, I., Michiue, H., Takeuchi, T., Tomizawa, K., Matsui, H. and Futaki, S. (2009) Enhanced intracellular delivery using arginine-rich peptides by the addition of penetration accelerating sequences (Pas). J Control Release. **138**, 128-133
23 Lukanowska, M., Howl, J. and Jones, S. (2013) Bioportides: bioactive cell-penetrating peptides that modulate cellular dynamics. Biotechnol J. **8**, 918-930
24 He, L., Sayers, E. J., Watson, P. and Jones, A. T. (2018) Contrasting roles for actin in the cellular uptake of cell penetrating peptide conjugates. Sci Rep. **8**, 7318
25 Patel, S. G., Sayers, E. J., He, L., Narayan, R., Williams, T. L., Mills, E. M., Allemann, R. K., Luk, L. Y. P., Jones, A. T. and Tsai, Y.-H. (2019) Cell-penetrating peptide sequence and modification dependent uptake and subcellular distribution of green florescent protein in different cell lines. Scientific Reports. **9**, 6298
26 Schindelin, J., Arganda-Carreras, I., Frise, E., Kaynig, V., Longair, M., Pietzsch, T., Preibisch, S., Rueden, C., Saalfeld, S., Schmid, B., Tinevez, J. Y., White, D. J., Hartenstein, V., Eliceiri, K., Tomancak, P. and Cardona, A. (2012) Fiji: an open-source platform for biological-image analysis. Nat Methods. **9**, 676-682
27 Humphries, W. H. t., Szymanski, C. J. and Payne, C. K. (2011) Endo-lysosomal vesicles positive for Rab7 and LAMP1 are terminal vesicles for the transport of dextran. PLoS One. **6**, e26626
28 Pu, J., Keren-Kaplan, T. and Bonifacino, J. S. (2017) A Ragulator-BORC interaction controls lysosome positioning in response to amino acid availability. J Cell Biol. **216**, 4183-4197
29 Sayers, E. J., Cleal, K., Eissa, N. G., Watson, P. and Jones, A. T. (2014) Distal phenylalanine modification for enhancing cellular delivery of fluorophores, proteins and quantum dots by cell penetrating peptides. Journal of Controlled Release. **195**, 55-62
30 Birch, D., Christensen, M. V., Staerk, D., Franzyk, H. and Nielsen, H. M. (2017) Fluorophore labeling of a cell-penetrating peptide induces differential effects on its cellular distribution and affects cell viability. Biochim Biophys Acta Biomembr. **1859**, 2483-2494
31 Zhang, F., Wang, S., Yin, L., Yang, Y., Guan, Y., Wang, W., Xu, H. and Tao, N. (2015) Quantification of epidermal growth factor receptor expression level and binding kinetics on cell surfaces by surface plasmon resonance imaging. Anal Chem. **87**, 9960-9965
32 Yu, X., Ghamande, S., Liu, H., Xue, L., Zhao, S., Tan, W., Zhao, L., Tang, S. C., Wu, D., Korkaya, H., Maihle, N. J. and Liu, H. Y. (2018) Targeting EGFR/HER2/HER3 with a Three-in-One Aptamer-siRNA Chimera Confers Superior Activity against HER2(+) Breast Cancer. Mol Ther Nucleic Acids. **10**, 317-330
33 Watkins, C. L., Schmaljohann, D., Futaki, S. and Jones, A. T. (2009) Low concentration thresholds of plasma membranes for rapid energy-independent translocation of a cell-penetrating peptide. Biochem J. **420**, 179-189
34 Futaki, S. and Nakase, I. (2017) Cell-Surface Interactions on Arginine-Rich Cell-Penetrating Peptides Allow for Multiplex Modes of Internalization. Acc Chem Res. **50**, 2449-2456

35 Wang, Z., Chen, Y., Liu, E., Gong, J., Shin, M. C. and Huang, Y. (2014) CPP-mediated protein delivery in a noncovalent form: proof-of-concept for percutaneous and intranasal delivery. Protein Pept Lett. **21**, 1129-1136
36 Carter, E., Lau, C. Y., Tosh, D., Ward, S. G. and Mrsny, R. J. (2013) Cell penetrating peptides fail to induce an innate immune response in epithelial cells in vitro: implications for continued therapeutic use. Eur J Pharm Biopharm. **85**, 12-19
37 Dinca, A., Chien, W. M. and Chin, M. T. (2016) Intracellular Delivery of Proteins with Cell-Penetrating Peptides for Therapeutic Uses in Human Disease. Int J Mol Sci. **17**, 263
38 Mussbach, F., Franke, M., Zoch, A., Schaefer, B. and Reissmann, S. (2011) Transduction of peptides and proteins into live cells by cell penetrating peptides. J Cell Biochem. **112**, 3824-3833
39 Chaudhary, P., Thamake, S. I., Shetty, P. and Vishwanatha, J. K. (2014) Inhibition of triple-negative and Herceptin-resistant breast cancer cell proliferation and migration by Annexin A2 antibodies. Br J Cancer. **111**, 2328-2341
40 Tan, X., Thapa, N., Liao, Y., Choi, S. and Anderson, R. A. (2016) PtdIns(4,5)P2 signaling regulates ATG14 and autophagy. Proc Natl Acad Sci U S A. **113**, 10896-10901
41 Dittmann, K., Mayer, C., Fehrenbacher, B., Schaller, M., Kehlbach, R. and Rodemann, H. P. (2010) Nuclear EGFR shuttling induced by ionizing radiation is regulated by phosphorylation at residue Thr654. FEBS Lett. **584**, 3878-3884
42 Gerhart, J., Thevenin, A. F., Bloch, E., King, K. E. and Thevenin, D. (2018) Inhibiting Epidermal Growth Factor Receptor Dimerization and Signaling Through Targeted Delivery of a Juxtamembrane Domain Peptide Mimic. ACS Chem Biol. **13**, 2623-2632
43 Palm, C., Jayamanne, M., Kjellander, M. and Hallbrink, M. (2007) Peptide degradation is a critical determinant for cell-penetrating peptide uptake. Biochim Biophys Acta. **1768**, 1769-1776
44 Trehin, R., Nielsen, H. M., Jahnke, H. G., Krauss, U., Beck-Sickinger, A. G. and Merkle, H. P. (2004) Metabolic cleavage of cell-penetrating peptides in contact with epithelial models: human calcitonin (hCT)-derived peptides, Tat(47-57) and penetratin(43-58). Biochem J. **382**, 945-956
45 Birch, D., Christensen, M. V., Staerk, D., Franzyk, H. and Nielsen, H. M. (2018) Stereochemistry as a determining factor for the effect of a cell-penetrating peptide on cellular viability and epithelial integrity. Biochem J. **475**, 1773-1788
46 Jamasbi, E., Ciccotosto, G. D., Tailhades, J., Robins-Browne, R. M., Ugalde, C. L., Sharples, R. A., Patil, N., Wade, J. D., Hossain, M. A. and Separovic, F. (2015) Site of fluorescent label modifies interaction of melittin with live cells and model membranes. Biochim Biophys Acta. **1848**, 2031-2039
47 Jansen, C., Tobita, C., Umemoto, E. U., Starkus, J., Rysavy, N. M., Shimoda, L. M. N., Sung, C., Stokes, A. J. and Turner, H. (2019) Calcium-dependent, non-apoptotic, large plasma membrane bleb formation in physiologically stimulated mast cells and basophils. J Extracell Vesicles. **8**, 1578589
48 van den Bogaart, G., Guzman, J. V., Mika, J. T. and Poolman, B. (2008) On the mechanism of pore formation by melittin. J Biol Chem. **283**, 33854-33857
49 Cabrera, M. P., Alvares, D. S., Leite, N. B., de Souza, B. M., Palma, M. S., Riske, K. A. and Neto, J. R. (2011) New insight into the mechanism of action of wasp mastoparan peptides: lytic activity and clustering observed with giant vesicles. Langmuir. **27**, 10805-10813
50 Hyun, S., Lee, Y., Jin, S. M., Cho, J., Park, J., Hyeon, C., Kim, K. S., Lee, Y. and Yu, J. (2018) Oligomer Formation Propensities of Dimeric Bundle Peptides Correlate with Cell Penetration Abilities. ACS Cent Sci. **4**, 885-893
51 Kristensen, M. and Nielsen, H. M. (2016) Cell-penetrating peptides as tools to enhance non-injectable delivery of biopharmaceuticals. Tissue Barriers. **4**, e1178369
52 Lemmon, M. A. and Schlessinger, J. (2010) Cell signaling by receptor tyrosine kinases. Cell. **141**, 1117-1134
53 Hedger, G., Sansom, M. S. and Koldso, H. (2015) The juxtamembrane regions of human receptor tyrosine kinases exhibit conserved interaction sites with anionic lipids. Sci Rep. **5**, 9198

54 Poon, I., Baxter, A. A., Lay, F. T., Mills, G. D., Adda, C. G., Payne, J. A., Phan, T. K., Ryan, G. F., White, J. A., Veneer, P. K., van der Weerden, N. L., Anderson, M. A., Kvansakul, M. and Hulett, M. D. (2014) Phosphoinositide-mediated oligomerization of a defensin induces cell lysis. Elife. **3**, e01808
55 Baxter, A. A., Poon, I. K. and Hulett, M. D. (2017) The lure of the lipids: how defensins exploit membrane phospholipids to induce cytolysis in target cells. Cell Death Dis. **8**, e2712
56 Moreno, M. and Giralt, E. (2015) Three valuable peptides from bee and wasp venoms for therapeutic and biotechnological use: melittin, apamin and mastoparan. Toxins (Basel). **7**, 1126-1150
57 Splith, K. and Neundorf, I. (2011) Antimicrobial peptides with cell-penetrating peptide properties and vice versa. Eur Biophys J. **40**, 387-397
58 Henriques, S. T., Melo, M. N. and Castanho, M. A. (2006) Cell-penetrating peptides and antimicrobial peptides: how different are they? Biochem J. **399**, 1-7

11. Tables

Table 1: Peptides and proteins used in this study.

Peptides	**Sequence**
L-EJP18	Ac-LFMRRRHIVRKRTLRRLL-NH_2
D-EJP18	Ac-lfmrrrhivrkrtlrrll-NH_2
Rh-L-EJP18	Rh-LFMRRRHIVRKRTLRRLL-NH_2
Rh-D-EJP18	Rh-lfmrrrhivrkrtlrrll-NH_2
L-R8	Ac-RRRRRRRR-NH_2
Rh-L-R8	Rh-RRRRRRRR-NH_2
r8-PAD	Ac-rrrrrrrrGGklaklakklaklakGC-NH_2
Proteins	
eGFP-R8	His_6-*eGFP*-RRRRRRRR
eGFP-EJP18	His_6-*eGFP*-LFMRRRHIVRKRTLRRLL
eGFP	His_6-*eGFP*

Capital letters represent L amino acids, lower case represents D amino acids, Rh = tetramethylrhodamine, Ac = acyl, NH_2 = amide and italics *eGFP* represent full length enhanced green fluorescent protein.

Table 2: IC50 cell viability values for the four cell lines tested

Cell line	L-EJP18 IC50 (µM)	D-EJP18 IC50 (µM)
HeLa	63.7±7.9	12.2±1.3
MDA-MB-231	63.0±20.3	28.9±2.5
KG1a	20.2±1.5	15.8±2.9
A431	> 100	22.6±8.2

Values calculated from viability curves in Figure 1. Values represent the mean of the repeats +/- SEM, n = 3, N = 3.

Table 3: Juxtamembrane and transmembrane (TM) peptide sequences of 58 human RTKs

Class	RTK	Upstream TM (5 aa)	Juxtamembrane Sequence (20 aa)
I	EGFR	IGLFM	RRRHIVRKR**T**LRRLLQEREL
I	ErbB2	FGILI	KRRQQKIRKYTMRRLLQETE
I	ErbB3	GGTFL	YWRGRRIQNKRAMRRYLERG
I	ErbB4	FAVYV	RRKSIKKKRALRRFLETELV
II	InsR	IYLFL	RKRQPDGPLGPL**Y**ASSNPE**Y**
II	IGF1R	LYVFH	RKRNNSRLGNGVLYASVNPE
II	IRR	ALGFF	YGKKRNRTLYASVNPEYFSA
III	PDGFRα	LVVIW	KQKPRYEIRWRVIESISPDG
III	PDGFRβ	LIILI	MLWQKKPR**Y**EIRWKVIESVS
III	KIT	MILTY	K**Y**LQKPM**Y**EVQWKVVEEING
III	CSF1R	LLLLY	KYKQKPK**Y**QVRWKIIESYEG
III	FLT3	TLLIC	HKYKKQFR**Y**E**S**QLQMVQVTG
IV	VEGFR1	LTLFI	RKMKRSSSEIKTDYLSIIMD
IV	VEGFR2	LLVII	LRTVKRANGGELKTG**Y**LSIV
IV	VEGFR3	LLLLI	FCNMRRPAHADIKTGYLSII
V	FGFR1	SVIVY	KMKSGTKKSDFHSQMAVHKL
V	FGFR2	TVILC	RMKNTTKKPDFSSQPAVHKL
V	FGFR3	AVTLC	RLRSPPKKGLGSPTVHKISR
V	FGFR4	LAGLY	RGQALHGRHPRPPATVQKLS
VI	PTK7	GLMFY	CKKRCKAKRLQKQPEGEEPE
VII	NTRK1	LLLVL	NKCGRRNKFGINRPAVLAPE
VII	NTRK2	MLFLL	LARHSKFGMKGPASVISNDD
VII	NTRK3	LFVMI	NKYGRRSKFGMKGPVAVISG
VIII	ROR1	FFICV	CRNNQKSSSAPVQRQPKHVR
VIII	ROR2	CLFFL	VCMCRNKQKASASTPQRRQL
IX	MuSK	ITTLY	CCRRRKQWKNKKRESAAVTL
X	MET	FFLWL	KKRKQIKDLG**S**ELVRYDARV
X	Ron	TALVF	SYWWRRKQLVLPPNLNDLAS
XI	Axl	ALFLV	HRRKKETRYGEVFEPTVERG
XI	Tyro3	LALIL	LRKRRKETRFGQAFD**S**VMAR
XI	Mer	SLAIR	KRVQETKFGNAFTEED**S**ELV
XII	TIE1	LLTLV	CIRRSCLHRRRTFTYQSGSG
XII	TIE2	AFLII	LQLKRANVQRRMAQAFQNVR
XIII	EphA1	GILVF	RSRRAQRQRQQRQRDRATDV
XIII	EphA2	VGFFI	HRRRKNQRARQ**S**PEDV**Y**FSK
XIII	EphA3	YVLIG	RFCGYKSKHGADEKRLHFGN
XIII	EphA4	AAFVI	SRRRSKYSKAKQEADEEKHL
XIII	EphA5	IGVLL	SGSCCECGCGRASSLCAVAH
XIII	EphA6	LFFLI	TGRCQWYIKAKMKSEEKRRN
XIII	EphA7	MVFGF	IIGRRHCGYSKADQEGDEEL
XIII	EphA8	LLLIC	KKRHCGYSKAFQDSDEEKMH
XIII	EphA10	VMSVL	AIWRRPCSYGKGGGDAHDEE
XIII	EphB1	ISIVC	SRKRAYSKEAVYSDKLQHYS
XIII	EphB2	VIAIV	CNRRGFERADSEYTDKLQHY
XIII	EphB3	VIAIV	CLRKQRHGSDSEYTEKLQQY
XIII	EphB4	IVVAV	LCLRKQSNGREAEYSDKHGQ
XIII	EphB6	AITVL	AVVFQRKRRGTGYTEQLQQY
XIV	Ret	SAFCI	HCYHKFAHKPPISSAEMTFR
XV	RYK	AIILA	VLHLHSMKRIELDDSISASS
XVI	DDR1	IALML	WRLHWRRLLSKAERRVLEEE
XVI	DDR2	VIILW	RQFWQKMLEKASRRMLDDEM
XVII	ROS	LTFVW	HRRLKNQKSAKEGVTVLINE
XVIII	LMTK1	LMLAC	LCCKKGGIGFKEFENAEGDE
XVIII	LMTK2	IVLIA	NCVSCCKDPEIDFKEFEDNF
XVIII	LMTK3	LLTCL	CCKRGDVGFKEFENPEGEDC
XIX	LTK	VLILV	KQKKWQGLQEMRLPSPELEL
XIX	ALK	IMIVY	RRKHQELQAMQMELQSPE**Y**K
XX	STYK1	GVILW	LFIREQRTQQQRSGPQGIAP

Positively charged amino acids in green, negatively charged amino acids in red, **bold** represents phosphorylated or putative phosphorylated amino acids (data collected from Uniprot).

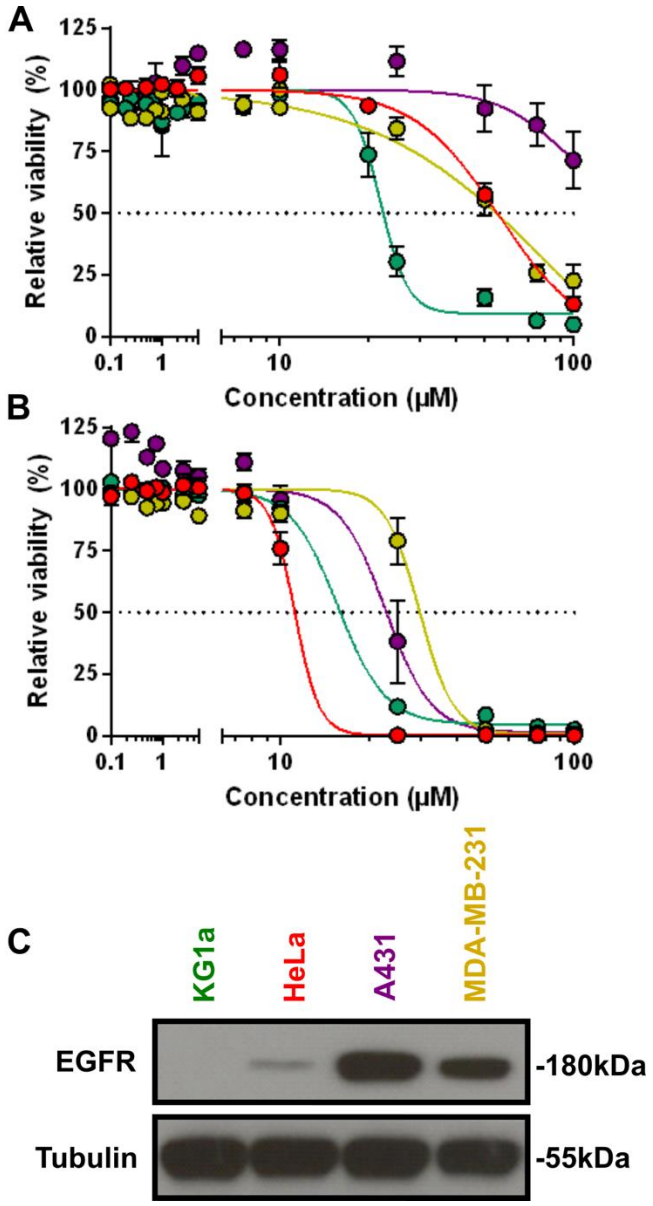

12.

Figure 1: Viability and EGFR expression of cell lines incubated with L- and D-EJP18

Viability of HeLa cells (red), MDA-MB-231 cells (yellow), KG1a cells (green) and A431 (purple) following incubation with L-EJP18 (A) or D-EJP18 (B) for 24 h in CM. The dotted line depicts 50 % viable cells. Mean ± SEM, n = 3, N = 3. (C) Representative western blot showing the relative expression of EGFR in the four cell lines normalised by total protein concentration.

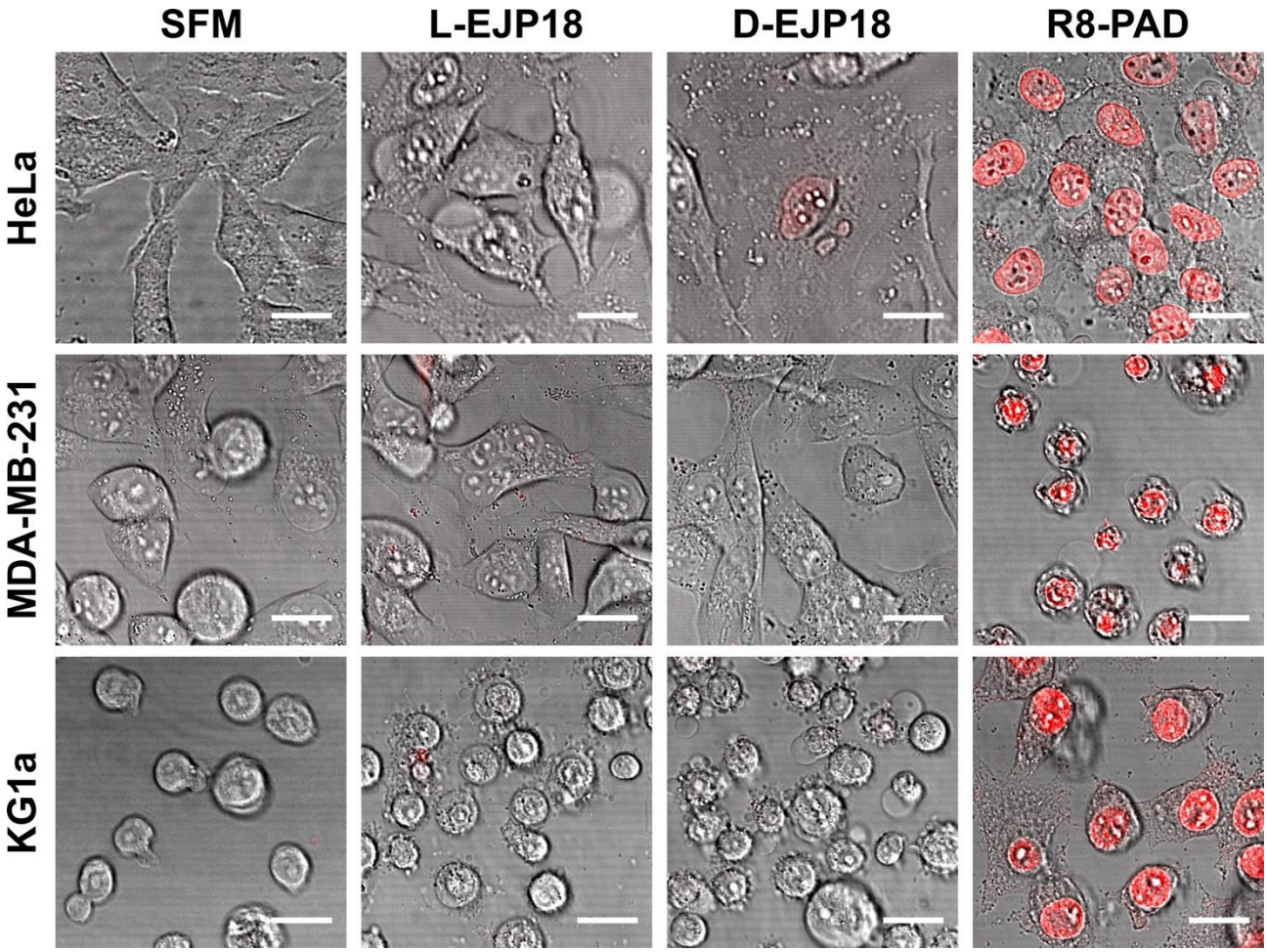

Figure 2: Morphological changes in KG1a, HeLa and MDA-MB-231 cells incubated with L- and D-EJP18. Cells were incubated with/without 20 µM CPP for 1 h in SFM in the presence of DRAQ7 (red). Representative images are from two identical experiments in different passages. Scale bars = 20 µm. For one-hour time lapse movies see Supplementary Information, M1 to M12.

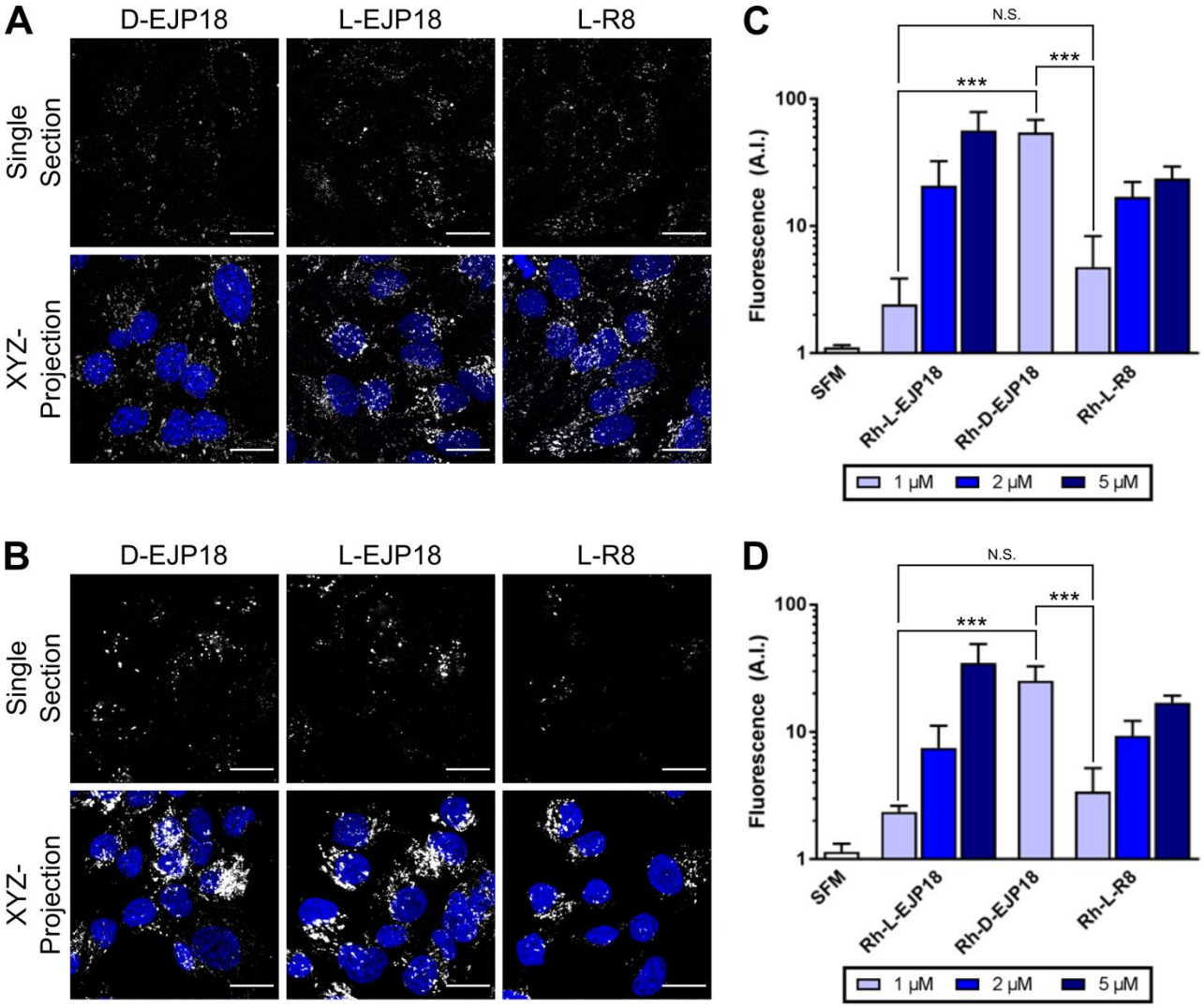

Figure 3: Uptake of Rh-EJP18 in HeLa and MDA-MB-231 cells

HeLa (A) and MDA-MB-231 (B) cells were incubated with 2 µM Rh-labelled L-EJP18, D-EJP18 or L-R8 (green) in SFM for 1 h prior to washing and imaging. Scale bars = 20 µm. Relative uptake of Rh-L-EJP18, Rh-D-EJP18 and Rh-L-R8 into HeLa (C) and MDA-MB-231 (D) cells. Cells were treated with test solution (1-5 µM in SFM) for 1 h at tissue culture conditions and subsequently analysed by flow cytometry. Fluorescence values are a mean of the mean geometric mean from three independent experiments performed in triplicate. Mean ± SEM, n = 3, N = 3. For example histograms see Supplementary Information, Figure S3, for additional comparative statistics from the ANOVA see Supplementary Information, Tables 1 and 2.

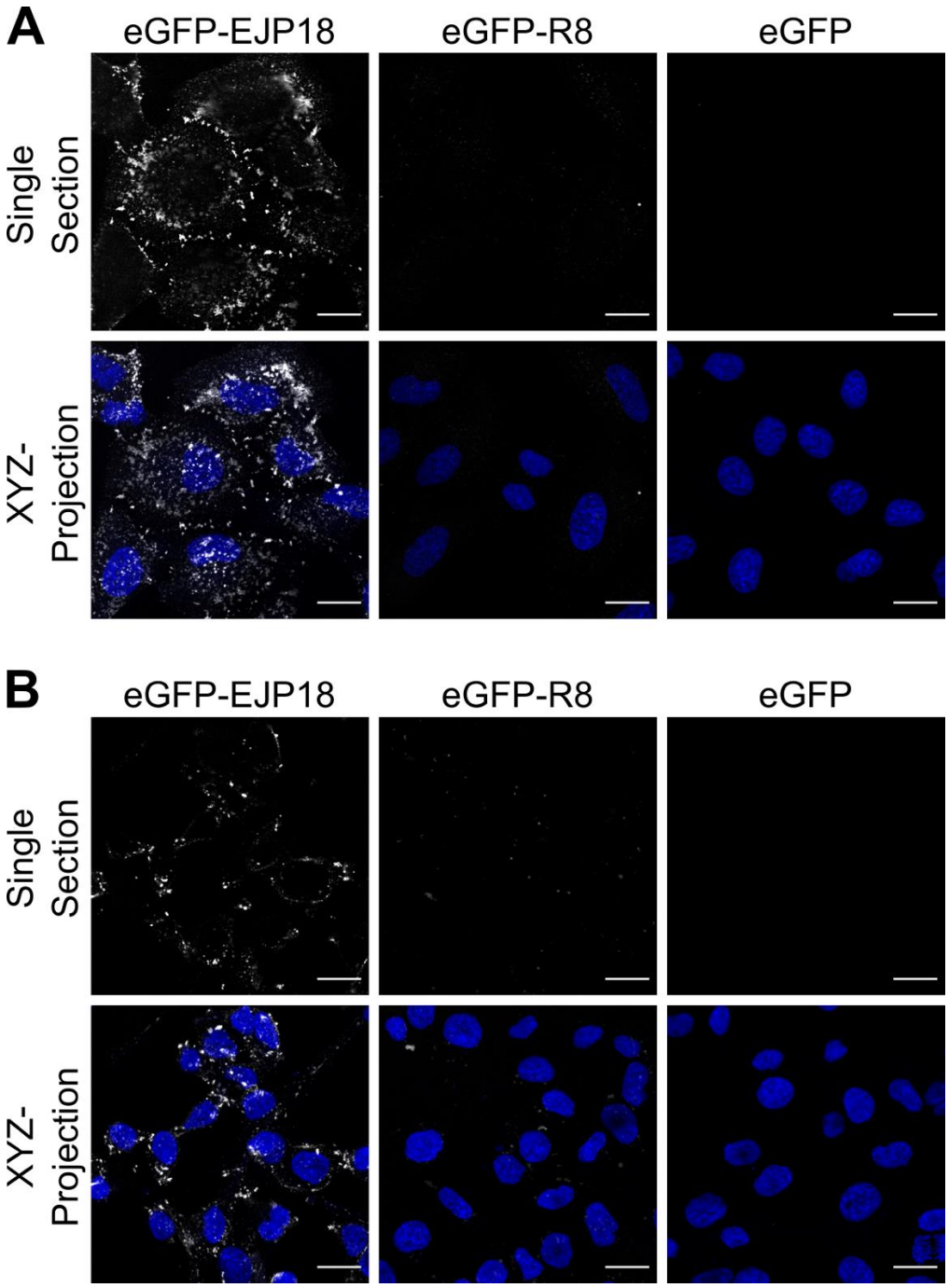

Figure 4: Cell uptake of eGFP by EJP18 and L-R8

HeLa (A) and MDA-MB-231 (B) cells were incubated with 2 µM eGFP-EJP18, eGFP-R8 or eGFP in SFM for 1 h prior to washing and imaging by confocal microscopy. Scale bar = 20 µm.

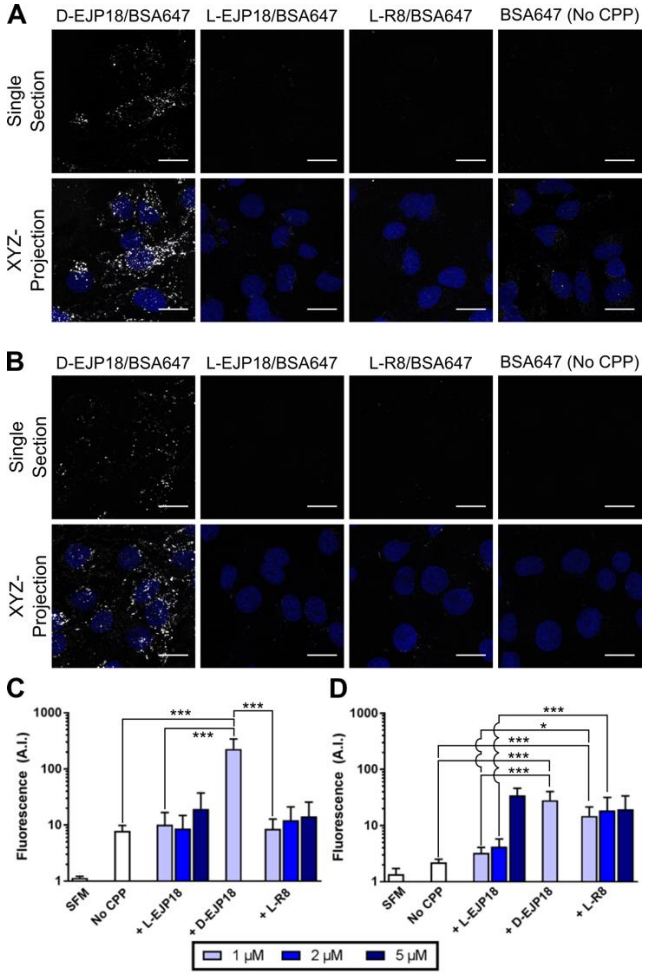

Figure 5: Cell uptake of peptide-BSA complexes in cells

Complexes of CPP and BSA were formed by mixing 8 µM L-EJP18, D-EJP18 or L-R8 (unlabelled) with 240 nM BSA-Alexa647 (molar ratio CPP:BSA 100:3) in distilled water for 30 min at room temperature. Complexes were subsequently diluted 1 part in 4 in SFM, to produce final peptide and protein concentrations of 2 µM and 60 nM respectively, and incubated with (A) HeLa or (B) MDA-MB-231 cells for 1 h prior to washing and imaging. Scale bars = 20 µm. Relative uptake of L-EJP18, D-EJP18 and L-R8 complexed with BSA-Alexa647 into (C) HeLa and (D) MDA-MB-231 cells. Cells were treated with tested peptides (1-5 µM in SFM) for 1 h at tissue culture conditions and subsequently analysed by flow cytometry. Fluorescence values are a mean of the mean geometric mean from three independent experiments performed in triplicate. Mean ± SEM, n = 3, N = 3. For example histograms see Supplementary Information, Figure S8, for additional comparative statistics from the ANOVA see Supplementary Information, Tables 3 and 4.

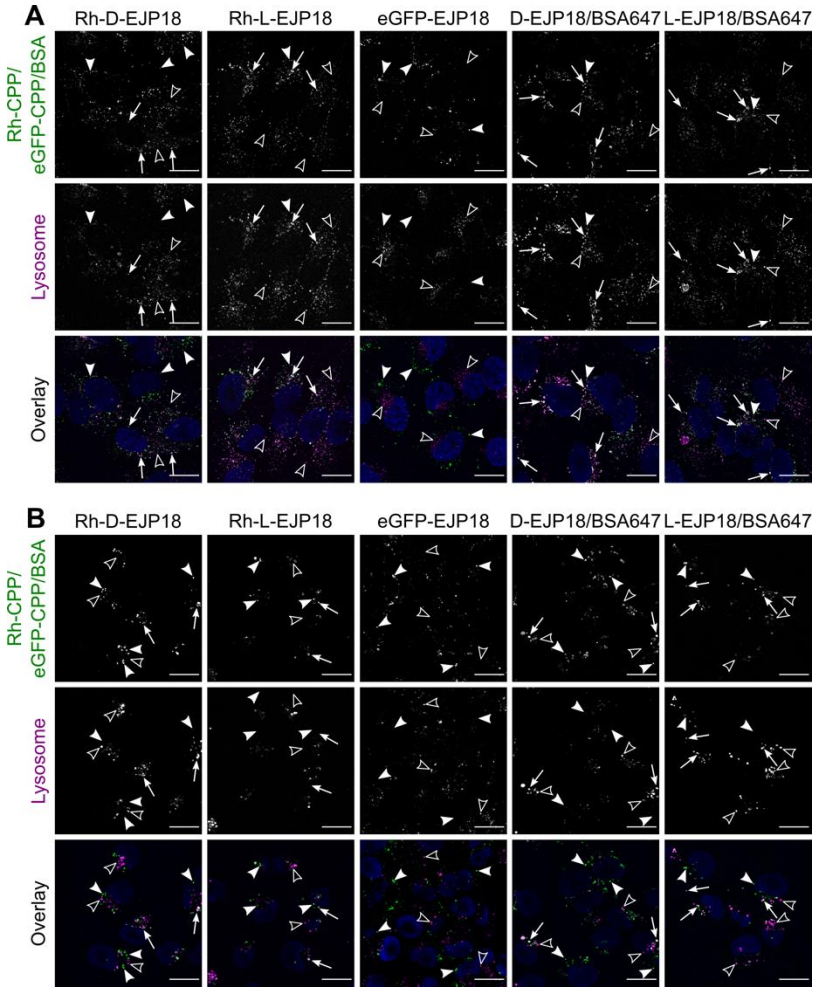

Figure 6: Differential rates of endocytic traffic to lysosomes for small molecule or protein cargo delivered by EJP18

HeLa (A) and MDA-MB-231 (B) cells, with the lysosomes pre-loaded with fluorescent dextran (magenta), were incubated with 2 µM rhodamine labelled L- or D-EJP18, 2 µM L- or D-EJP18 complexed with 60 nM BSA-Alexa 647 or 2 µM eGFP-EJP18 (all in green) in SFM for 1 h. Cells were chased by incubating in CM for a further 1 h before imaging in the presence of Hoechst 33342. Scale bar = 20 µm. Arrows indicate colocalised cargo and lysosomal dextran, solid arrows indicate non-colocalised cargo and hollow arrow heads indicate non-colocalised lysosomal dextran. Image intensities have been adjusted so that differences in colocalisation can be more evenly compared. All images are single sections. Enlarged overlays can be found as Supplementary Information, Figure S9.

Supplementary Movie M1: HeLa cells were incubated in serum free medium (SFM) for 1 h and imaged in presence of DRAQ7, a marker for membrane permeability.

Supplementary Movie M2: HeLa cells were incubated with 20 µM L-EJP18 in SFM for 1 h and imaged in presence of DRAQ7, a marker for membrane permeability.

Supplementary Movie M3: HeLa cells were incubated with 20 µM D-EJP18 in SFM for 1 h and imaged in presence of DRAQ7, a marker for membrane permeability.

Supplementary Movie M4: HeLa cells were incubated with 20 µM R8-PAD in SFM for 1 h and imaged in presence of DRAQ7, a marker for membrane permeability.

Supplementary Movie M5: MDA-MB-231 cells were incubated in serum free medium (SFM) for 1 h and imaged in presence of DRAQ7, a marker for membrane permeability.

Supplementary Movie M6: MDA-MB-231 cells were incubated with 20 µM L-EJP18 in SFM for 1 h and imaged in presence of DRAQ7, a marker for membrane permeability.

Supplementary Movie M7: MDA-MB-231 cells were incubated with 20 µM D-EJP18 in SFM for 1 h and imaged in presence of DRAQ7, a marker for membrane permeability.

Supplementary Movie M8: MDA-MB-231 cells were incubated with 20 µM R8-PAD in SFM for 1 h and imaged in presence of DRAQ7, a marker for membrane permeability.

Supplementary Movie M9: KG1a cells were incubated in serum free medium (SFM) for 1 h and imaged in presence of DRAQ7, a marker for membrane permeability.

Supplementary Movie M10: KG1a cells were incubated with 20 µM L-EJP18 in SFM for 1 h and imaged in presence of DRAQ7, a marker for membrane permeability.

Supplementary Movie M11: KG1a cells were incubated with 20 µM D-EJP18 in SFM for 1 h and imaged in presence of DRAQ7, a marker for membrane permeability.

Supplementary Movie M12: KG1a cells were incubated with 20 µM R8-PAD in SFM for 1 h and imaged in presence of DRAQ7, a marker for membrane permeability.